Primary surface ruptures of the great Himalayan earthquakes in 1934 and 1255

S. N. Sapkota [1], L. Bollinger [2*], Y. Klinger [3], P. Tapponnier [4], Y. Gaudemer [3], and D. Tiwari[1].
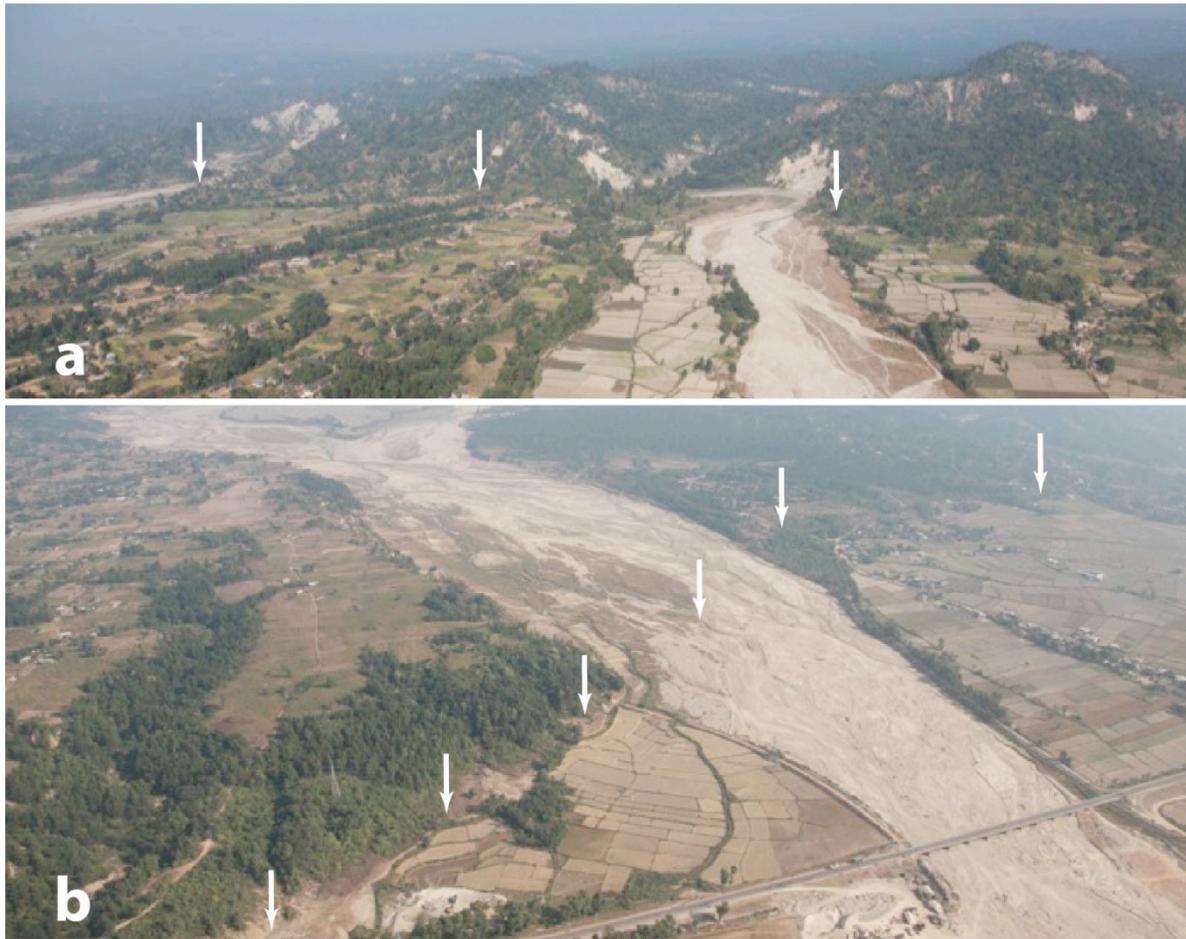
Affiliations:

[1]Department of Mines and Geology, National Seismic Center, Kathmandu, Nepal.

[2]CEA, DAM, DIF, F-91297 Arpajon, France.

[3]Institut de Physique du Globe de Paris, CNRS, Paris, France.

[4]Earth Observatory of Singapore, Nanyang Technological University, Singapore.
*Correspondence to: Laurent.bollinger@cea.fr .

Supplementary Figure S1: Oblique helicopter views, from south and southwest, respectively, of cumulative escarpments along Patu and Bardibas Thrusts. a/ Northern branch of MFT (Patu Thrust), across Sir river outlet (right) NNW of Bardibas. Patu Thrust trace (white arrows) follows sharp contact between deeply incised white Siwalik sandstones in background and inset terraces in foreground. b/ Southern branch of MFT (Bardibas Thrust, white arrows) across Ratu river just east of Bardibas. High hanging-wall strath terrace on west bank of river stands ≈ 45 m above footwall. Note how modern, grass-covered terrace only a few meters above river on same bank restricts, by about half, width of present flood-plain on hanging wall.

Supplementary Information S1:

Supplementary Figure S2: Close-up view of F1 splays and drag-folded stratigraphy in frontal part of river cut photomosaic (Interpretation in Fig. 3c).

a/ Sir river west bank geomorphology and Quaternary geology

Evidence for active thrusting was more limited on the west bank of the Sir river, where we found direct exposure of only one young thrust exhumed by incision and lateral cutting (F3, on T2/T1 riser, Fig.2). The exact location of this thrust was confirmed by excavating a 15 m-long, 3 m-deep auxiliary trench at the foot of the riser (A-Tr, Fig. 2). The $\approx 25°$ N-dipping thrust (F3) emplaces a thin wedge of white Siwaliks capped by 30 cm of pebbles/cobbles (T2h) onto oxidized conglomerates (lateral equivalent of U6-10). But no datable material was found in T2h. On T1 and T2, the thrust emergence is marked by a shift from thick conglomerate layers on the footwall to only $\approx$ 20-30 cm-thick veneers of pebbles on the hanging-wall - a transition from fill to strath-terrace. A similarly sharp transition between abraded Siwaliks upstream and gravels downstream is apparent across the river floodplain, corresponding to a change from dark to light hue visible on satellite images in many river valleys that cross the MFT.

Inside the river meander, there are perched, southward-tilted, higher-level terraces (T3h, T4h) and beheaded, hanging channels north of the most frontal thrust, whose trace we mapped precisely in the field to follow the geological contact between white Siwalik sandstones and buff-colored Quaternary conglomerates (Fig. 2). But the lowest terrace surfaces (T2h, T1) have been reworked by large modern floods short-circuiting the interior of the meander. On T2h for instance, straight, recent primary channels are still outlined by thicker grass and bush-lines (Fig. 2). Finally, the west-bank geomorphology is more complex, due to deep incision by lateral tributaries, and the original landforms have been modified by the construction of canals and man-made roads and paths (Fig. 2).

b/ Nature and ages of youngest Sir river east bank deposits

On the east bank of the river and hanging wall of F1, the wedge at the base of the cumulative escarpment thickens northwards to ≈ 3 m (Fig. 3). In section along the refreshed river-cut face, much of the wedge body and toe (U1) are composed of fine, soft, light-colored sand/silt deposits thinning southwards into a distal taper, implying they are mostly derived from colluvial wash, but there is one flat, thin bed of small pebbles, about one third up-section above the basal unconformity. This indicates that some of the wedge material, probably including also a few thin, well-stratified sand layers, is composed of fluvial overbank deposits.

The proximal part of the wedge, just beneath and south of F3, is mostly composed of poorly sorted fluvial pebbles and cobbles mixed with irregular blocks or fragments of white Siwalik sandstones and siltstones (Fig. 3A). Although a few 20° S-dipping pebble layers are visible at the base, bedding in this part of the wedge is undefined overall, which implies an origin by gravity-driven collapse of upthrust Siwaliks and unconsolidated fluvial conglomerates from the steep south face of the escarpment. This in turn implies that ^{14}C ages from the charcoal samples collected in the wedge ought to show dispersion, with dates in part older than the age of emplacement. Note however that, even if interpreted as reworked, the oldest sample (Fig. 3A), with a calibrated age of 1420-1640 AD (SIR09-17, Table S1), is at most 600 years old. Reworking may have occurred also due to fluvial transport and redeposition. For instance, of the 5 samples retrieved from the footwall sand lenses in U5 (Fig. 3B, C), two (SIR09-04 and SIR09-11, Table S1) have ages (2460-2140 BC, 1740-1510 BC) that are significantly older than the other three, whose clustered age-range is 1450-1130 BC.

c/ 1833 earthquake

The 26 august 1833 event (Fig. 4) is a less likely candidate than the Bihar Nepal earthquake. Its magnitude (Mw = 7.6) was much less, and its macroseismic area (1° farther north and west), 3 times smaller than that of the 1934 event. Its epicenter was located north of Kathmandu, south of Langtang Himal [1]. It thus seems more plausible that it ruptured primarily the ramp south of the high range [2], with slip perhaps mostly confined to the middle crust.
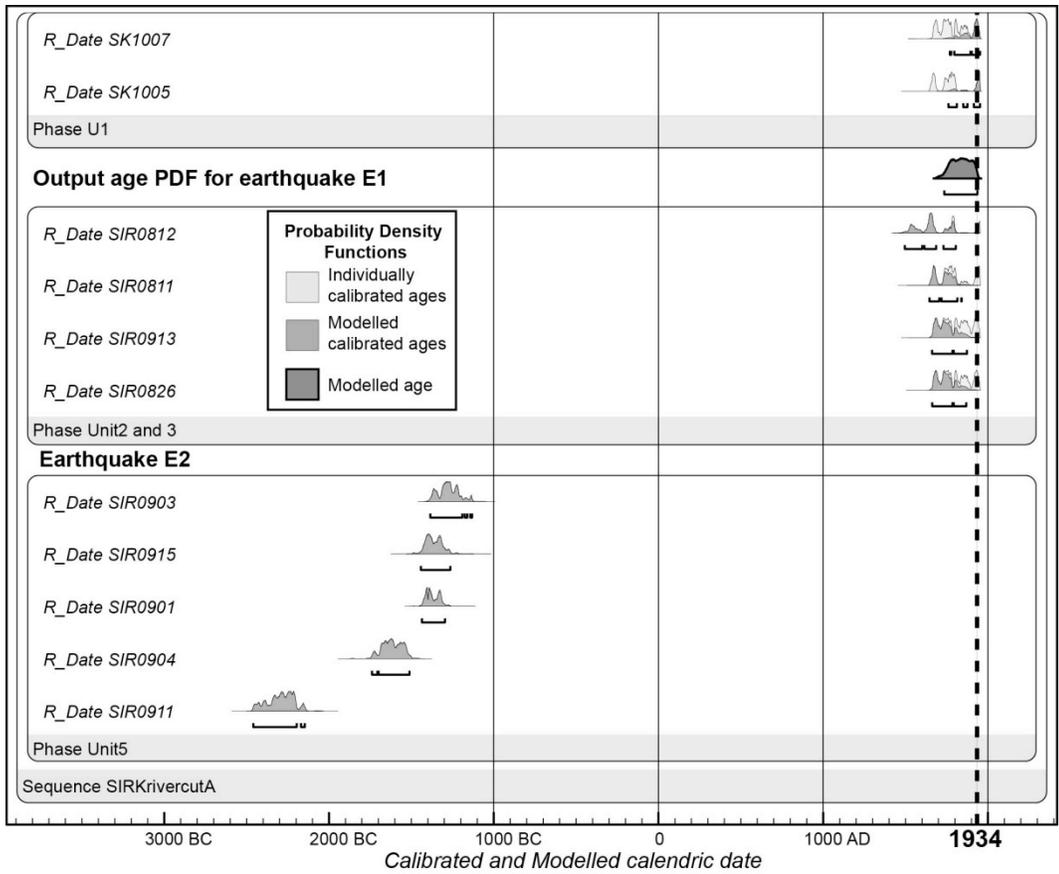
Supplementary Figure S3A: OxCal model (version 4.1), [3], of timing constraints for surface-rupturing seismic events on F1, along Sir rivercut face (see discussion in Methods).
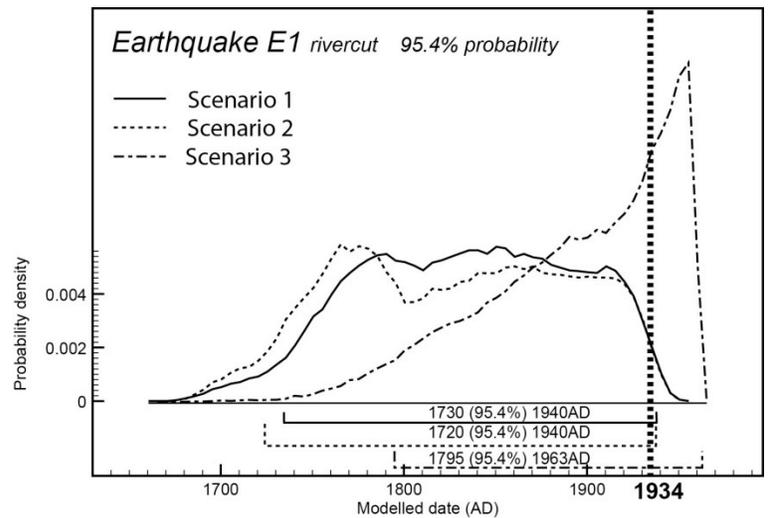
Supplementary Figure S3B: Comparison of Probability Density Functions (PDF) for age of last event (E1) along Sir rivercut face according to 3 deposition scenarios discussed in (Methods). Most probable age falls between 1720 and 1963 AD, at 95,4% confidence level, including date of 1934 earthquake. Calibration curves are from [4, 5].
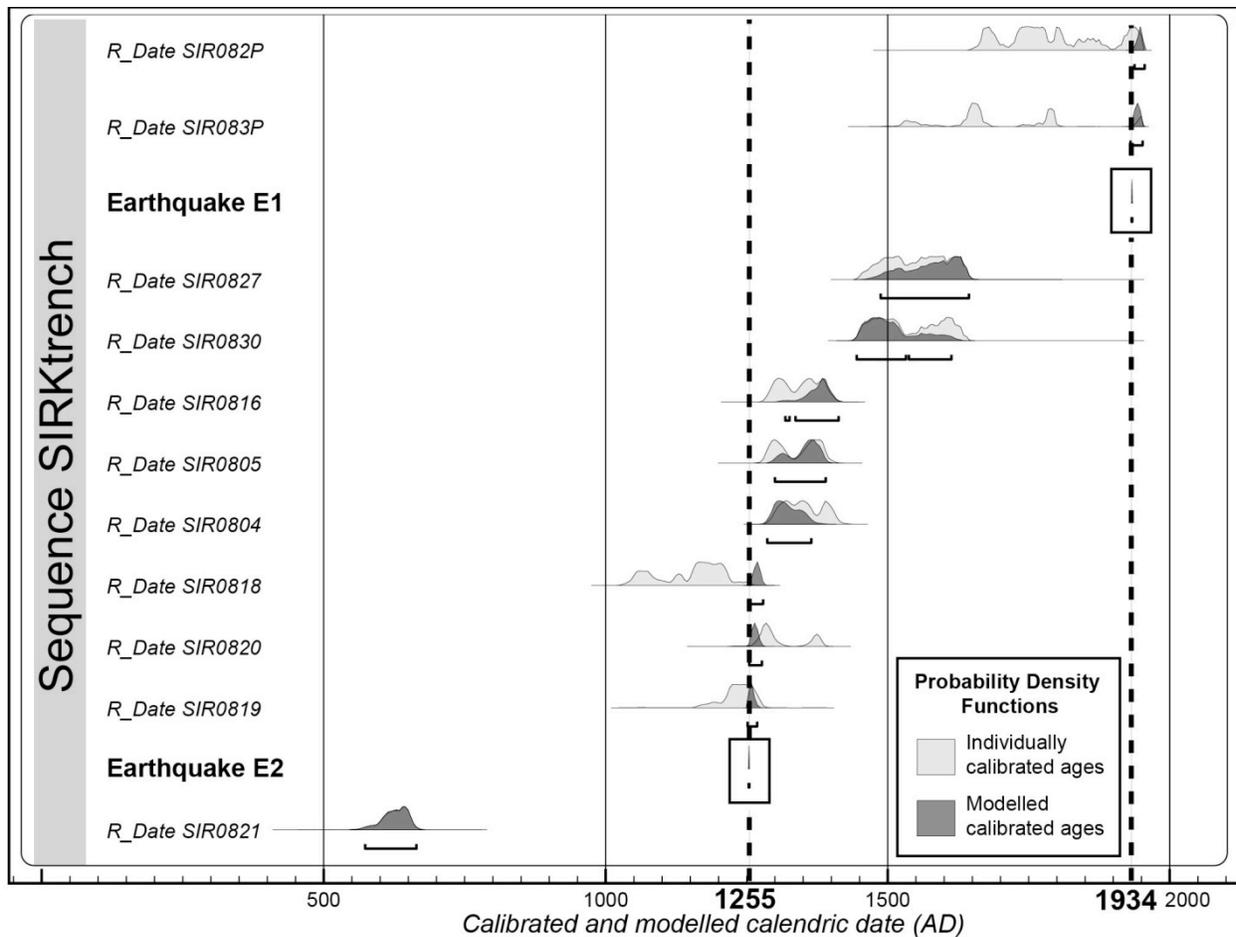
Supplementary Figure S3C: OxCal model (version 4.1), [3], of timing constraints for surface-rupturing seismic events in Sir river main trench (see discussion in Methods). 1255 AD and 1934 AD dates are used as a priori inputs. .

Supplementary Information S2:

Maximum rupture extent and magnitude of 1934 earthquake:

On the west bank of the Mahara river, ≈ 5 km west of the Sir river (star, Fig. 1B), paleo-seismological evidence was found for only one large medieval event, in ≈ AD 1100 (nowhere mentioned in historical catalogues or texts), but not for the 1934 earthquake [6]. The two events were thus interpreted to be very different, the former qualifying as a giant earthquake (M > 8.8), with an open-ended return period (> 912 yrs). However, the lack of surface rupture in 1934 was not inescapably demonstrated: two thrusts emerging near the base of a 4m-high scarp next to the river bank were not sealed by dated deposits. Besides, since some detrital charcoals may be inherited, one cannot exclude the possibility that the otherwise unknown 1100 AD "Mahara river" event might in fact be the AD 1255 earthquake, which would reconcile the paleo-seismic histories of these two adjacent sites. In Dharan, just east of the Sardu river (Fig. S4), no clear surface scarp crosses the large fan upon which the city is built. Beveling by man-made construction cannot be

ruled out, however. Moreover, the overall geomorphology suggests that the MFT steps south, east of the river.

Hence, one cannot exclude that the 1934 surface rupture extended eastwards past Dharan, and westwards past the Mahara river, perhaps reaching a length on order of 200-250 km (Fig. 5). This might imply a magnitude Mw ≈ 8.4 larger than that most commonly adopted [e.g. 7] and close to the uppermost possible bound [8], which would contribute to reduce the mismatch between the cumulative moment released by Himalayan earthquakes and the accrued inter-seismic moment deficit [9, 10]. In any event, one should perhaps now regard seismic hazard in eastern Nepal to be somewhat less than along other stretches of the mega-thrust, rather than maximum, which might be the case if the ultimate event had been a giant earthquake in AD 1100 [6]. The actual risk of an impending great MFT earthquake might be significantly more on either side of the 1934 rupture (Fig. 5), south of Sikkim and/or Bhutan for instance, or in central Nepal, perhaps especially east of the source of the great 1505 earthquake [9].

Supplementary Figure S4: a- Top Left / East looking view of T2 (foreground) and T4 (background) terrace surfaces on MFT hangingwall in Tintale creek, on West bank of Charnath Khola. T2 and T4 are strath terraces standing 6.0+/-0.5 m and 15+/-1 m above the creek and dated at 1875 +/-30 AD and 870 +/- 30 AD, respectively. This is consistent with co-seismic uplift in both the 1934 and 1255 events. b- Bottom Left/ North looking view of free-faced scarp of MFT at Mirchaya. S. Sapkota stands for scale on uplifted strath gravels 5+/-1 m above the footwall. c- Top Right / Northwest looking view of steep, south-facing 6+/-1 m-high MFT scarp in forest near Khairban. d-Bottom Right/ ≈ 4.5 m-high free-faced incision into terrace layers in Sardu Khola river-bed, on MFT hanging wall just west of Dharan. F. Perrier stands for scale in front of exposed stack of 5 main fluvial units including ≈ 1 m of older, oxidized, consolidated conglomerates capped by ≈ 3m of modern, grey colored, unconsolidated gravel/pebble/cobble layers. Strong incision starts just north of MFT trace on west side of river channel, while it is negligible south of MFT. By comparison with Sir Khola, this implies relatively recent co-seismic uplift, even though rigorous dating has not yet been undertaken.

Supplementary Table S1: AMS Radiocarbon (^{14}C) dates from detrital charcoals collected from Sir river-cut and main trench.

Unit[a]	Sample Number	SUERC Laboratory Code[b]	Measured Radiocarbon Age (years B.P.)[c]	δ^{13}C value [d]	Calibrated Ages (calendric, 2σ)
Rivercut					
U0	SIR08-03	25771	Modern (postbomb)	-27.9	
U1$_{aF3}$	SK10-07	34605	150 +/- 30	-30.7	AD 1660-1960
U1$_{aF3}$	SK10-05	34598	195 +/- 30	-27.5	AD 1640-1960
U1$_H$	SIR09-17	28375	415 +/- 40	-24.6	AD 1420-1640
U3$_H$	SIR09-13	28373	145 +/- 40	(-25.0)	AD 1660-1960
U3$_F$	SIR08-26	23691	150 +/- 35	-25.6	AD 1660-1960
U3$_H$	SIR08-11	23683	185 +/- 35	-29.1	AD 1640-1960
U3$_H$	SIR08-12	23960	245 +/- 45	-25.0	AD 1490-1960
U5$_F$	SIR09-03	27999	3015 +/- 30	(-25.0)	BC 1390-1130
U5$_F$	SIR09-15	28374	3095 +/-40	(-25.0)	BC 1450-1260
U5$_F$	SIR09-01	27998	3100 +/- 30	-27.8	BC 1440-1290
U5$_F$	SIR09-04	28371	3335 +/- 45	-26.3	BC 1740-1510
U$_{uF4}$	SIR08-25	23690	3430 +/- 35	-25.5	AD 1880-1630
U5$_F$	SIR09-11	28372	3830 +/- 40	-26.7	BC 2460-2140
Trench					
U1t	SIR08-2P	23694	165 +/- 35	-24.4	AD 1660-1960
U1t	SIR08-3P	23695	245 +/- 35	-27.1	AD 1520-1960
U3t	SIR08-27	25778	340 +/- 35	-27.9	AD 1460-1650
U3t	SIR08-30	25779	365 +/- 35	(-25.0)	AD 1440-1640
U3t	SIR08-16	25772	625 +/- 35	-27.4	AD 1280-1400
U5t	SIR08-22	23961	955 +/- 45	-25.0	AD 990-1190
U6t	SIR08-04	23680	600 +/- 35	-27.6	AD 1290-1410
U6t	SIR08-20	25773	695 +/- 35	-27.6	AD 1250-1390
U6t	SIR08-18	23684	875 +/- 35	-26.3	AD 1040-1260
U6t	SIR08-19	23685	795 +/- 35	-27.1	AD 1170-1280
U7t	SIR08-05	23681	645 +/- 35	-25.8	AD 1280-1400
U7t	SIR08-39	23938	955 +/- 40	-25.0	AD 990-1180
U11t	SIR08-21	25777	1415 +/- 35	-25.8	AD 570-665

a -See rivercut and trench logs for stratigraphic unit designations
b -All samples have been dated by Accelerator Mass Spectrometry (AMS) measured at the Scottish Universities Environmental Research Centre (SUERC) AMS facility. Each number corresponds to the laboratory code for each sample.
c -Conventional Radiocarbon years B.P. relative to 1950 AD (with 1σ confidence level including counting statistics as well as reference standard, blank and random machine errors).
d -Parentheses denote samples for which values are unavailable and assumed to be -25.0
e -Calendric dates were calibrated using the atmospheric calibration curve IntCal09 for the Northern Hemisphere [4].

References

[1]. Cattin, R., Avouac, J.-P. Modeling mountain building and the seismic cycle in the Himalaya of Nepal. *J. Geophys, Res.* **105**, 13389-13407 (2000).

[2]. Bilham, R. Location and magnitude of the 1833 Nepal earthquake and its relation to the rupture zones of contiguous great Himalayan earthquakes *Curr. Sci.* **69**, 101-128 (1995).

[3]. Bronk Ramsey, C. Deposition models for chronological records. *Quat. Sci. Rev.* **27**, 42-60 (2008).

[4]. Reimer, P. J., et al., IntCal09 and Marine09 radiocarbon age calibration curves, 0–50,000 years cal BP. *Radiocarbon* **51**, 1111-1150 (2009).

[5]. Hua, Q., Barbetti, M. Review of tropospheric bomb C-14 data for carbon cycle modeling and age calibration purposes. *Radiocarbon* **46**, 1273-1298 (2004).

[6]. Lavé J. et al., Evidence for a Great Medieval Earthquake (~1100 A.D.) in the Central Himalayas of Nepal. *Science* **307**, 1302-1305 (2005).

[7]. Ambraseys, N.N., Douglas, J. Magnitude calibration of north Indian earthquakes, *Geophys. Jour. Int.* **159**, 165-206 (2004).

[8]. Molnar, P., Denq, Q. Faulting associated with large earthquakes and the average rate of deformation in central and eastern Asia. *Jour. Geophys. Res.* **89**, 6203-6227 (1984).

[9]. Bilham, R., Gaur, V.K., Molnar, P. Earthquakes - Himalayan seismic hazard. *Science* **293**, 1442-1444 (2001).

[10]. Ader, T.et al., Convergence rate across the Nepal Himalaya and interseismic coupling on the Main Himalayan Thrust: Implications for seismic hazard. *J. Geophys. Res.* **117**, B04403 (2012).